

---

# RCT: RESOURCE CONSTRAINED TRAINING FOR EDGE AI

---

A PREPRINT

Tian Huang<sup>1</sup>, Tao Luo<sup>1</sup>, Ming Yan<sup>1</sup>, Joey Tianyi Zhou<sup>1</sup>, and Rick Goh<sup>1</sup>

<sup>1</sup>Institute of High Performance Computing, A\*STAR

<sup>1</sup>{huang\_tian, lu\_tao, yan\_ming, joey\_zhou, gohsm}@ihpc.a-star.edu.sg

March 29, 2021

## ABSTRACT

Neural networks training on edge terminals is essential for edge AI computing, which needs to be adaptive to evolving environment. Quantised models can efficiently run on edge devices, but existing training methods for these compact models are designed to run on powerful servers with abundant memory and energy budget. For example, quantisation-aware training (QAT) method involves two copies of model parameters, which is usually beyond the capacity of on-chip memory in edge devices. Data movement between off-chip and on-chip memory is energy demanding as well. The resource requirements are trivial for powerful servers, but critical for edge devices. To mitigate these issues, We propose Resource Constrained Training (RCT). RCT only keeps a quantised model throughout the training, so that the memory requirements for model parameters in training is reduced. It adjusts per-layer bitwidth dynamically in order to save energy when a model can learn effectively with lower precision. We carry out experiments with representative models and tasks in image application and natural language processing. Experiments show that RCT saves more than 86% energy for General Matrix Multiply (GEMM) and saves more than 46% memory for model parameters, with limited accuracy loss. Comparing with QAT-based method, RCT saves about half of energy on moving model parameters.

## 1 Introduction

Edge computing emerges as an attractive alternative to cloud computing, for its advantages in data privacy, response latency and energy saving for data transmissions [1]. Deep learning-based intelligence, as another growing trend, have started to change many aspects of people’s lives. Well trained deep learning models are able to achieve record-breaking predictive performance [2, 3, 4], but we have witnessed increasing demand for the model to learn in-situ, for the purpose of personalisation or adaptation to evolving environment. Comparing to cloud-based deep learning framework, training a neural network on edge device reflects the very idea of edge computing, and benefits from energy savings in data transmission, low response latency and enhanced privacy.

Quantisation is a popular technique that improves energy efficiency and speed of a neural network. There are many free and commercialised tools for converting well-trained neural network to a quantised one. But training a quantised model is tricky. Quantisation-aware training (QAT) [5] is a big family of methods that matches the requirement of in-situ learning. Most of QAT-based training methods are based on the assumption that resources like memory and energy are abundant.

QAT-based methods involve two copies of model parameters during training, as shown in Figure 1a. (1) At first stage, floating-point model travels from memory to processor for quantisation. (2),(3) Then quantised model takes part in inference and generate loss. (4) At the stage of model update, the floating-point model has to travel from memory to processor again such that the gradients can be added to the floating point parameters. The update is usually followed by another write-back to the memory. Such training method is not friendly for edge AI from two aspects. First, on-chip memory of edge devices (e.g. cache or buffer in a processor) is usually limited in size such that the floating-point model parameters have to stay in off-chip memory (e.g. DRAM), which is much slower than on-chip memory. Second, data

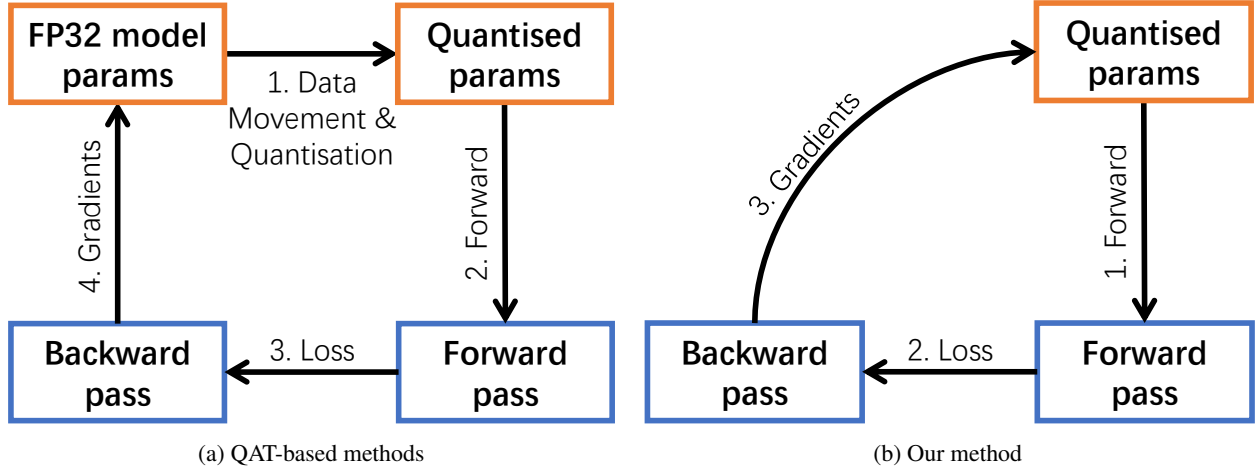


Figure 1: Comparison between QAT-based methods and RCT. (a) QAT-based methods involve two copies of model parameters. (b) Our method RCT only keeps a quantised model.

movement is energy demanding. Battery-powered edge devices may not have enough energy to support two copies of a model and frequent data movement between off-chip memory and processors.

As shown in Figure 1b, if we only keep a quantised model, we save the memory for floating-point parameters. Since a quantised model is usually compact enough to stay in on-chip memory throughout training, we can also save energy for related data movement.

The challenge is that with quantised parameters alone, a model does not always learn effectively. A model with low-precision parameters may learn without difficulty at the beginning of the training process. As training loss and gradients decrease along with the training progress, quantisation underflow happens more often in the model update step, and slows down or even puts a stall to the training progress. Allocating more bitwidth could mitigate the underflow issue and sustain the overall training efficiency.

Based on this observation, we propose a heuristic method called **Resource Constrained Training (RCT)**, which applies a per-layer metric that reflects how often quantisation underflow is happening. By evaluating the metrics, RCT understands how effective a layer learns with given precision. RCT allocates more bitwidth to the parameters of a layer if underflow happens very often. The per-layer bitwidth of a model changes dynamically throughout the training process. Below shows a list of our contributions:

- We propose a heuristic training method RCT, which is aware of the training progress and adjusts per-layer bitwidth dynamically to save energy for training.
- RCT only keeps quantised parameters. In this way, we reduce the memory requirements for model parameters in training.
- RCT provides an application specific hyper-parameter that achieves trade-off between training energy, memory usage, and accuracy.

RCT finds the per-layer bitwidth configuration that helps the model learn effectively with quantised parameters only. It benefits edge devices that have to learn in-situ frequently after deployment. In the experiment we apply RCT to representative CNN models on image classification tasks. We also evaluate RCT with representative NLP applications. Comparing to non-quantisation baseline, RCT saves more than 86% energy for General Matrix Multiply (GEMM) and saves more than 46% memory for model parameters, with limited accuracy loss. Comparing with other QAT-based methods, RCT saves more than half of memory for model parameters and related energy for transmitting model parameters.

## 2 Related Work

There are two kinds of popular quantisation methods, Quantisation-aware training (QAT) and post-training quantisation [5]. QAT emulates inference-time quantisation during training, which helps in maintaining accuracy as compared to 16-bit or 32-bit floating-point baselines. The recent progress in QAT has allowed the realization of results comparable to

a baseline for as low as 2–4 bits per parameter [6, 7, 8, 9, 10, 11, 12] and show decent performance even for single bit (binary) parameters [13, 14, 15, 16, 17, 18]. There are QAT-based methods that efficiently exploit various processing units [19, 20, 21, 22, 23, 24], as well as the ones that allocate per-layer bitwidth [25, 26, 27, 28] to improve the performance of a quantised model. Apart from image related applications, QAT-based methods has also been applied to Natural Language Processing (NLP). [23, 27, 13, 24]

QAT-based methods can train a quantised model. However, these QAT-based methods involves two copies of model parameters, as they are based on the assumption that the machine for training has abundant memory and electricity supply. This is usually not true for edge devices. We propose RCT, which only has one copy of model parameters. It saves memory, as well as the energy for related data movement.

The post-training quantisation [29, 30, 31, 32, 33, 34] converts a well-trained model into quantised one. By definition, post-training quantisation methods convert models but do not train them. It does not meet the requirements of in-situ learning, in which quantised models continue to evolve on edge devices.

Imposing *sparsity* in neural network is an effective way of compression [35, 36, 37, 38, 39]. In general, sparsity comes in the cost of irregular memory access patterns and unbalanced computation workload, [40, 41] which raise resource utilisation issues on a resource constrained devices. Other techniques, e.g. *Knowledge Distillation* [42], *Low-rank Factorisation* [43, 44], *Fast Convolution* [45], save memory and/or energy significantly for inference. These methods only conduct compression but do not train the model after it is compressed.

### 3 Resource Constrained Training

In this section we describe the details of RCT. We explain why QAT-based methods involve two copies of model parameters, and how RCT can train effectively with only one quantised model.

#### 3.1 Motivation

Low precision integer arithmetic is more efficient than a floating point arithmetic in terms of energy and memory, but quantisation magnifies the underflow issue. [5] Equation 1 shows the update process of a weight in fp32 format:

$$w_{ij} := w_{ij} - lr * g_{ij} \quad (1)$$

$w_{ij}$  is the  $j$ -th weight of  $i$ -th layer,  $lr$  is the learning rate,  $g_{ij}$  is the corresponding gradient of the  $w_{ij}$ . Ideally, at each training step, a weight changes by  $lr * g_{ij}$ . As we apply  $k$ -bit quantisation to a tensor of weights, too small changes cannot be represented by the weight. We refer to this minimum resolution as  $\epsilon$ , which is formalised as follow:

$$\epsilon_i = \frac{\max(W_i) - \min(W_i)}{2^k - 1} \quad (2)$$

$W_i$  is a tensor of weights of  $i$ -th layer.  $k$  is the precision, or the bitwidth for the tensor. The updates of a weight  $w_{ij}$  is regulated by  $\epsilon_i$ , which can be formalised as the following equation:

$$w_{ij} := w_{ij} - \left\lfloor \frac{lr * g_{ij}}{\epsilon_i} \right\rfloor * \epsilon_i \quad (3)$$

As a result,  $lr * g_{ij}$  is quantised to discrete states, which is equivalent to that of  $w_{ij}$ .  $lr * g_{ij}$  has to be at least larger than  $\epsilon_i$ , otherwise quantisation underflow happens. For high precision training (e.g. 32-bit)  $\epsilon$  is small,  $lr * g_{ij}$  is larger than  $\epsilon_i$  for most of cases. As the precision decreases,  $\epsilon_i$  increases, quantisation underflow happens more often, putting higher resistance on weights updating.

Gradient is the horse power that drives the training process forward. Low-precision training put restrictions on the horse power and slow down the training process. We have the observation that in low precision network, gradients vanishes quicker than that of a network with higher precision. This is because quantisation underflow happens more often in low precision model and guides the model into local minima. Some of layers have larger  $\epsilon$  and are harder to be updated than others. As the training loss decreases, These layers with larger  $\epsilon$  suffer more quantisation underflow than before, stepping onto a slippery slope. As the training process moves forward, quantisation underflow freezes more parameters, driving the training into a dead state.

Through the observation, we understand that mitigating the negative effect of quantisation underflow is critical to the training progress. Next we aim to find out how often quantisation underflow happens to a quantised layer.

### 3.2 Metrics for Underflow

QAT-based methods keep an fp32 model in order to avoid underflow, in the cost of memory usage, energy for data movement and additional training iterations. We aim to find low precision configurations that save memory and energy at the same time. The key is to understand how often quantisation underflow happens to a layer, We propose a metric called  $Gavg$ , which is formalised as Equation 4.

$$Gavg_i = \frac{1}{N_i} \sum_{j=0}^{N_i} \left| \frac{g_{ij}}{\epsilon_i} \right| \quad (4)$$

$N_i$  represents the number of parameters in a tensor,  $Gavg_i$  indicates how large a gradient is related to the minimum resolution of parameters in  $i$ -th layer. The larger the  $Gavg$  is, the less likely the parameters remains unchanged during model update. If  $Gavg$  approaches zero, that means the layer suffers serious quantisation underflow problem and does not update for most of times. The bitwidth is the key to prevent  $Gavg$  from approaching zero. A higher bitwidth leads to lower  $\epsilon$  and higher  $Gavg$ , which means the parameters are easier to update.

Although we use weights to describe the concept of quantisation underflow and metrics,  $Gavg$  applies to other parameters that need to be learned during training, e.g. bias, the clipping point of activation and gradient. In the metric  $Gavg$ , we do not include other factors like learning rate or momentum in the metric so that user can use other training tricks or sophisticated optimisers on top of our training method.

### 3.3 Bitwidth Adjustment Policy

The metric  $Gavg$  is a measurement for balancing requirements between training energy, memory usage, and accuracy. It is well known that bitwidth is directly related to the energy, memory and accuracy. Using fixed bitwidth across the whole network may not meets the requirement of each layer. On comparison, a single threshold for  $Gavg$  is able to produce different bitwidth configuration according to the distribution of parameters and their gradients.

We propose a bitwidth adjustment policy based on the metric  $Gavg$ . We start with a naive policy, which is to make sure that  $Gavg$  of all layers are within a pre-defined range. A C-styled description of the policy is presented below.

---

#### Algorithm 1: Bitwidth Adjustment Policy

---

**input** :  $k_{0...M-1}, Gavg_{0...M-1}, T_{min}, T_{max}$ ,

**output** :  $k_{0...M-1}$

```

1 for (  $i = 0; i < M; i = i + 1$  ) {
2   if (  $Gavg_i < T_{min} \ \&\& \ k_i < 32$  ) {
3      $k_i := k_i + 1;$ 
4   }
5   if (  $Gavg_i > T_{max} \ \&\& \ k_i > 2$  ) {
6      $k_i := k_i - 1;$ 
7   }
8 }
9 return  $k_{0...M-1};$ 

```

---

In Algorithm 1,  $k_{0...M-1}$  and  $Gavg_{0...M-1}$  represents the bitwidth and metrics of all  $M$  layers.  $T_{min}, T_{max}$  are the upper and lower limit. Algorithm 1 increase the bitwidth of a layer when its  $Gavg < T_{min}$  and decrease the bitwidth when  $Gavg > T_{max}$ . The lower limit ensures all layers learn effective, whereas the upper limit is for saving energy cost and memory usage on those parameters that are very easy to update (e.g. due to its small range or large gradients).

A typical workflow of RCT is described in Algorithm 2. A training starts with a low-precision model. The metrics evaluation and bitwidth adjustment happen between back propagation and model update. The evaluation and adjustment do not have to be done for each training iteration. A few times, say 10, in each epoch suffice to help the quantised training catch up with the progress of fp32 training.

We emphasise that the model parameters in RCT are quantised. QAT-based methods quantise the fp32 parameters in Forward propagation in Line 4 of Algorithm 2. In RCT, we only keep quantised parameters, so there is no parameter quantisation in forward pass at all.

Fig.2 demonstrates the trend of  $Gavg$  of two layers in a training with RCT.  $T_{min}$  is set to 1.0 in this demo. Layer A starts with a  $Gavg$  below  $T_{min}$ , indicating it suffers quantisation underflow. RCT allocates more bitwidth to lift the

**Algorithm 2:** Training with RCT

```

1 Initialise the model with low bitwidth, e.g.  $k = 8$  ;
2 for ( epoch = 0; epoch < 200; epoch ++ ) {
3   for ( i = 0; i < len(train_loader); i ++ ) {
4     Forward propagation ;
5     Loss back propagation ;
6     if ( i%INTERVAL == 0 ) {
7       Evaluate  $G_{avg}$  using Equation 4 ;
8       Adjust bitwidth using Algorithm 1 ;
9     }
10    Update model parameters ;
11  }
12 }
```

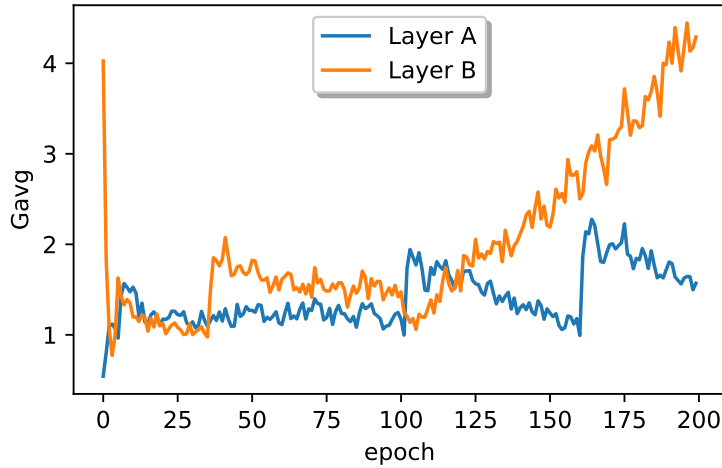


Figure 2:  $G_{avg}$  v.s. Epoch for two layers

$G_{avg}$  of layer A above the threshold. Layer B is very easy to update at the beginning. Whenever  $G_{avg}$  hits  $T_{min}$ , RCT allocates more bitwidth to ensure layer B learns effectively.  $T_{max}$  is set to  $+\infty$  in this demo. It is also possible to use  $T_{max}$  to reduce bitwidth for layers that do not suffer much from quantisation underflow.

Fig.3 demonstrates the distribution of bitwidth when we train WideResNet-28-10 on CIFAR100 dataset with RCT. The shade represents the 95% confidence interval. RCT adjusts the bitwidth of the each layer along with the training progress according to  $G_{avg}$ . Some layers are trained with lower bitwidth in early epochs and achieve solid energy savings. As the training progress move forward, the average of bitwidth increase gradually, indicates that RCT allocates more bitwidth to the layers with low  $G_{avg}$ .

Through Fig.3 we understand that RCT finds bitwidth configuration on the fly. It serves as a heuristic Neural Architecture Search method for edge devices. We start the training with an initial bitwidth of low precision, which is under-qualified with the target application. RCT will dynamically adjust the bitwidth of the network, and approaches the target accuracy with fewer energy.

### 4 Experiments

**Quantisation scheme** We apply linear quantisation scheme [46] to convert floating point numbers to into integers. The scheme is equivalent to an *affine mapping* of integers  $q$  to real numbers  $r$ . The formalised equation is shown as follows

$$r = S(q - Z)$$

.  $S$  and  $Z$  represent the scale and zero point of a group of values, or a tensor. All values in a tensor share one  $S$  and  $Z$ . Different tensors have their own  $S$  and  $Z$ . For  $k$ -bit quantisation,  $q$  has  $2^k$  possible discrete states. Additionally, we

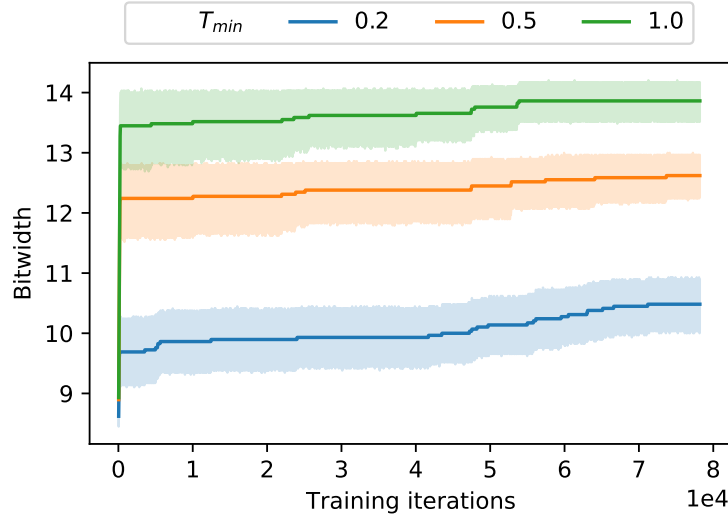


Figure 3: Layer-wise Bitwidth v.s. Epoch for WideResNet-28-10 on CIFAR100

apply Stochastic Rounding [47] to mitigate the errors introduced by quantisation. Unless specified, we use  $T_{min} = 1.0$  and  $T_{max} = 100.0$  for bitwidth adjustment policy in all the experiments.

**Energy Estimation** The energy for GEMM reported in this paper is simulated result. We assume the energy consumption of a quantised GEMM is proportional to that of a 32-bit counterpart. For example, a multiplication between two 16-bit operands consumes 25% energy compares to a 32-bit multiplication. This approximation is well supported by [48]. In this way, the reported energy is less dependent on the spec of a computing platform. We do not compare energy for computation with energy for data movement, because they are closely related to computer architecture as well as manufacturing process. We follow the rule of thumb that off-chip data movement is much more expensive than on-chip computation [48].

**Computing Infrastructure** We carry out all experiments on a general-purpose workstation, which is equipped with one Intel(R) Core(TM) i9-10900X CPU, 128-Gigabyte DDR4 memory and four NVIDIA Geforce RTX 2080 Ti graphics cards.

## 4.1 Image Classification

We evaluate the RCT with four datasets: CIFAR10, CIFAR100 [49], SVHN [50] and ImageNet [51]. Four popular backbones, ResNet-20, ResNet-110 [52], MobileNetV2 [53] and WideResNet [54], are included in the experiments. We replace all convolution layers and fully connected layers with our quantised version. Activation is quantised to 8-bit. This choice allows us to produce good energy savings without largely compromising the accuracy. The addition in fully connected layer is not quantised as they only make up for a fraction of the amount of memory and energy for training. We average over three runs of the experiment and report the results.

The quantised layers in these models are all initialised with 8-bit at the beginning of training. The result of training is not sensitive to the initial bitwidth. Please refer to Appendix for related experiments and analysis.

### 4.1.1 Savings in Energy

RCT saves energy when the model can learn with lower precision. The energy here refers to the energy for GEMM in inference. We demonstrate that, with RCT outperforms fixed precision training in accuracy and saves energy compared to floating point training. In this experiment, we use SGD to train WideResNet-28-10 on CIFAR100. We follow the training settings in [55]<sup>1</sup>. Fixed precision training and floating-point training is included as baselines in this experiment. Fig.4 shows the results of the experiment.

<sup>1</sup><https://github.com/uoguelph-mlrg/Cutout>

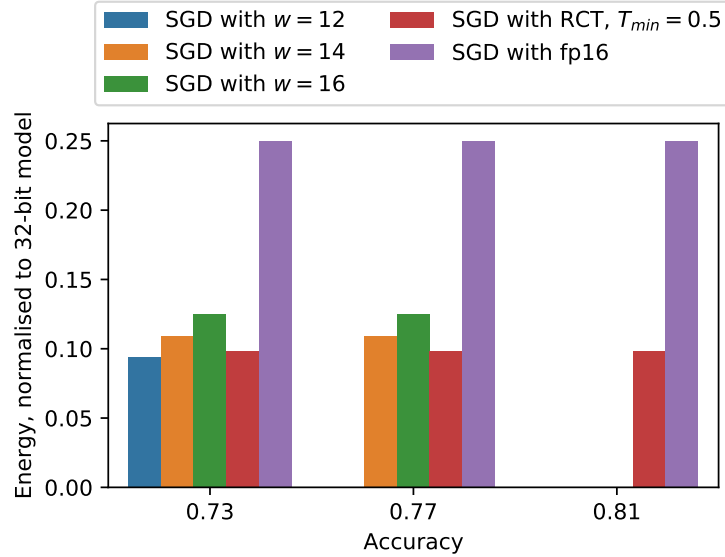


Figure 4: Training Energy v.s. Bitwidth for WideResNet-28-10 on CIFAR100

The SOTA accuracy achieved by SGD with fp32 is 81.59%. SGD with fp16 achieves similar accuracy with 25% of energy cost. SGD with RCT is able to achieve the same result with more than 90% savings in energy, about 15% more savings than SGD with fp16 does.

SGD with fixed precision  $w = 14$  and  $w = 16$  has energy cost that is just a few percent higher than RCT does. However they can only achieve 77% accuracy, 4% accuracy loss compared to the 81.59% SOTA accuracy. Similarly, SGD with  $w = 12$  consumes about the same energy as RCT does but only reaches 73% accuracy. The energy saving of fixed precision training comes in the cost of overfitting in the early stage of training and prevent the model from further improvement. We understand that the last few percents improvement in accuracy is usually the most energy consuming part in the whole training progress. This experiments suggests that RCT consumes less energy given the same target accuracy.

In Fig.4, RCT trains with  $T_{min} = 0.5$ . This hyper-parameter is application specific, which can be used as a trade-off between accuracy, memory and energy. Next we investigate the trade-off in the experiment. We train WideResNet-28-10 on CIFAR100 and ResNet-18 on CIFAR10. We follow the training setting in [55].

In Fig.5a, each point represents the results of a 150-epoch training using RCT. Threshold  $T_{min}$  for metric  $G_{avg}$  is ranging from 0.1 to 10. The dashed lines represents the SOTA accuracy. From the figure we know that for both models runs with  $T_{min} \geq 1.0$  result in accuracy very close to the SOTA accuracy.  $T_{min} = 0.5$  for ResNet-18 on CIFAR10 produces one more percent energy savings in the cost of accuracy loss of less than 1%. Overall,  $T_{min} = 0.5$  for both models provides at least 90% energy savings with accuracy loss no more than 1%.

#### 4.1.2 Savings in Memory

RCT only keeps quantised model parameters. The memory requirements for model parameters in training is reduced. Next we investigate the memory savings for model parameters achieved by RCT. We do not include memory for activation into the experiment, because this is not the focus of our method. One can use micro-batch technique [56] such that the memory requirements for activation is trivial comparing with model parameters.

The setting for Fig.5b is similar to Fig.5a except that x axis represents memory requirements for training, normalised to 32-bit models. From the figure we know that for both models runs with  $T_{min} \geq 1.0$  result in accuracy very close to the SOTA accuracy.  $T_{min} = 0.5$  for ResNet-18 on CIFAR10 produces one more percent memory savings in the cost of accuracy loss below 1%. Overall,  $T_{min} = 0.5$  for both models provides at least 65% memory savings with accuracy loss no more than 1%.

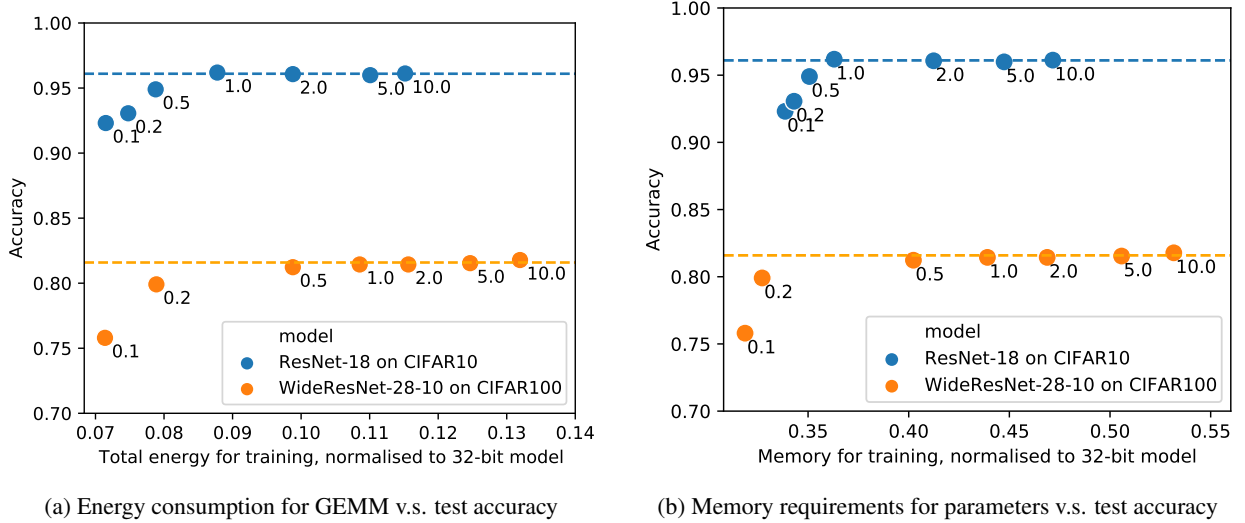


Figure 5: Image applications.  $T_{min}$  plays trade-off between scores and resource requirements. (a) Accuracy v.s. Memory for model parameters, normalised. (b) Accuracy v.s. Energy for GEMM, normalised

## 4.2 NLP tasks

We evaluate the RCT with Natural Language Processing (NLP) tasks. Pre-trained Transformer [57] based language models, such as BERT [58], have shown great improvement in many NLP tasks. In this experiment, we include text classification task set GLUE [59] and the question-answering task, SQuADv1.1 [60]. We employ BERT<sup>2</sup> as the backbone. We replace all embedding layers and fully connected layers with our quantised version. The precision of weights in these layers are all initialised as 8-bit at the beginning of training. Unless specified,  $(T_{min}, T_{max})$  is set to  $(1, 0, 100.0)$  for all experiments. Activation is quantised to 8-bit. The addition in fully connected layer is not quantised as they only make up for a fraction of the amount of memory and energy for training. We set batch size to 16 for GLUE and 12 for SQuADv1.1 and follow the rest of data processing and training methods presented in open-source library transformers<sup>3</sup>. We adopt random seeds in the experiment such that the reproducibility of the results is guaranteed.

Table 1: NLP performance

| Task      | Metric         | fp32  | RCT          | Bitwidth |
|-----------|----------------|-------|--------------|----------|
| CoLA      | Matthew’s corr | 56.53 | <b>57.29</b> | 18.0     |
| MRPC      | F1             | 88.85 | <b>90.20</b> | 17.9     |
| QNLI      | Accuracy       | 90.66 | <b>90.87</b> | 17.7     |
| QQP       | F1             | 87.49 | 86.74        | 17.6     |
| RTE       | Accuracy       | 65.70 | 65.34        | 18.8     |
| SST-2     | Accuracy       | 92.32 | 91.97        | 18.2     |
| STS-B     | Person corr.   | 88.64 | <b>88.78</b> | 17.9     |
| SQuADv1.1 | F1             | 88.46 | 87.62        | 18.2     |

We report our NLP experiment results in Table 1. The fp32 column is the score of a floating-point SGD method, which serves as a baseline. The RCT column shows the scores achieved by RCT method. RCT produces scores that are very close to the SOTA scores by the fp32 baseline method. The last column shows the averaged bitwidth of the quantised model at the end of RCT training.

Hyper-parameter  $T_{min}$  plays important roles in trade-off between the score and the resource required by the training process. Figure 6 shows the relation between them for BERT on SQuADv1.1.

In Figure 6, each point represents the result of a 2-epoch training process. The horizontal dotted line represents the score achieved by fp32 baseline. When  $T_{min} \geq 0.5$  the loss in score caused by RCT is always within 1%. When  $T_{min} < 0.5$

<sup>2</sup>bert-base-cased for GLUE, bert-base-uncased for SQuADv1.1

<sup>3</sup><https://github.com/huggingface/transformers/tree/v4.1.1>

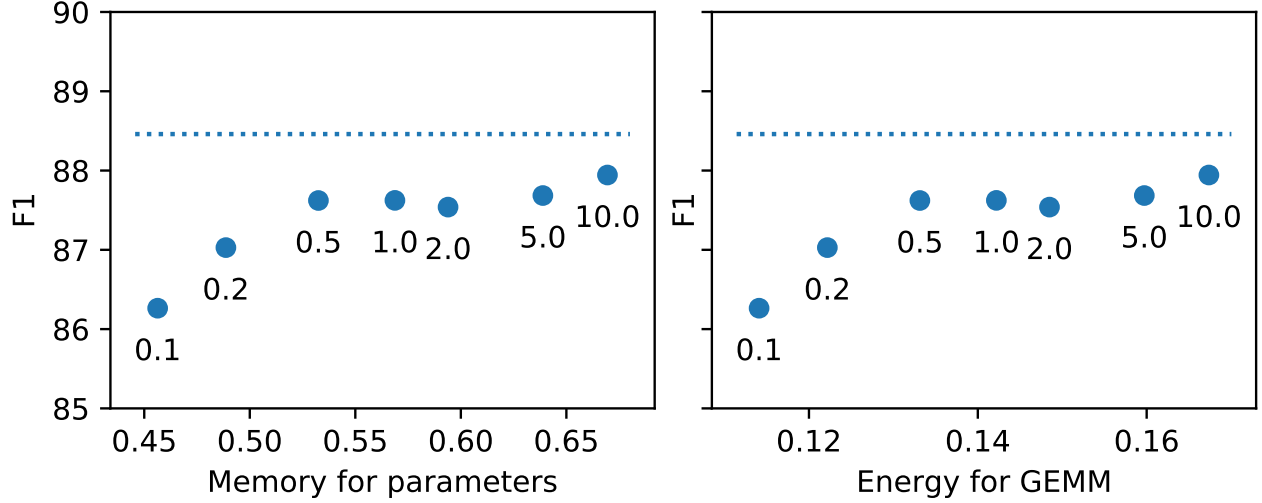


Figure 6: BERT on SQuADv1.1:  $T_{min}$  plays trade-off between scores and resource requirements. Left: F1 v.s. Memory for model parameters, normalised. Right: F1 v.s. Energy for GEMM, normalised

the score starts to drop gradually. This Figure together with Figure 5b and Figure 5a suggests that  $T_{min} = 0.5$  is a reasonable choice for various applications.

### 4.3 Comparison with Others

Table 2: Memory and Energy Comparison

| Method          | Model            | Dataset   | Accuracy loss <sup>a</sup> | Memory <sup>b</sup> | Energy <sup>c</sup> |
|-----------------|------------------|-----------|----------------------------|---------------------|---------------------|
| XNOR-Net [17]   | AlexNet          | ImageNet  | 12.4%                      | 32+1 bits           | -                   |
| TWN [12]        | ResNet-18        | ImageNet  | 3.6%                       | 32+3 bits           | 2.73                |
| QNN [20]        | ResNet-18        | ImageNet  | $\leq 1\%$                 | 32+8 bits           | 3.125               |
| WAGEUBN [22]    | ResNet-18        | ImageNet  | 3.9%                       | 24+8 bits           | 2.5                 |
| MP [19]         | ResNet-50        | ImageNet  | $\leq 1\%$                 | 32+16 bits          | -                   |
| PG [61]         | ShuffleNetV2     | ImageNet  | $\leq 1\%$                 | 32 bits             | 2.48                |
| Q8BERT [23]     | BERT             | GLUE      | $\leq 1\%$                 | 32+8 bits           | $\sim 2.22$         |
| Q8BERT [23]     | BERT             | SQuADv1.1 | $\leq 1\%$                 | 32+8 bits           | 2.20                |
| Q-BERT [27]     | BERT             | SQuADv1.1 | 2.3%                       | 32+3.7 bits         | 1.96                |
| BinaryBERT [13] | BERT             | SQuADv1.1 | $\leq 1\%$                 | 32+1 bits           | 1.81                |
| RCT             | MobileNetV2      | ImageNet  |                            | 12.1 bits           | -                   |
|                 | ShuffleNetV2     | ImageNet  |                            | 12.9 bits           | 1                   |
|                 | ResNet-18        | ImageNet  |                            | 12.8 bits           | 1                   |
|                 | ResNet-18        | CIFAR10   | $\leq 1\%$                 | 11.2 bits           | -                   |
|                 | WideResNet-28-10 | CIFAR100  |                            | 10.6 bits           | -                   |
|                 | BERT             | GLUE      |                            | $\sim 18$ bits      | 1                   |
|                 | BERT             | SQuADv1.1 |                            | 18.2 bits           | 1                   |

<sup>a</sup> The metrics for different tasks: Top1 accuracy for ImageNet, accuracy for CIFAR-10, F1 for SQuADv1.1, please refer to Table 1 for the metrics for GLUE task set.

<sup>b</sup> Memory for model parameters in training. We use averaged bitwidth as a model-independent indicator for memory requirements. For RCT, we report weighted average at the end of training.

<sup>c</sup> Energy for moving model parameters between off-chip memory and processor, normalised to the counterpart of RCT.

Table 2 shows the comparison between RCT and other representative training methods. Many of these methods involve two copies of model parameters during training, e.g., an fp32 copy and a quantised copy, thus have the form of  $32 + x$  bits in the memory column. RCT only involves one copy of model parameters, which has a better chance to fit into on-chip memory of a processor and stay inside throughout the training process.

In the case where the model parameters do not fit into on-chip memory, RCT still saves energy for data movement. We estimate that the energy for data movement is linearly proportional to the size of memory for model parameters. For example the energy cost by the training method for QNN is 3.125 times of what RCT requires, because  $\frac{32+8}{12.8} = 3.125$ . According to [48], DRAM operations, i.e., off-chip memory read/write, could be  $10^2 - 10^4$  times more expensive than on-chip operations do.

## 5 Discussion

### 5.1 Resource Efficient Hardware

Resource efficient hardware techniques are necessary for fully exploiting the benefit of RCT. The techniques here refer to the ability that a processing unit saves energy and memory according to the bit-width of operands, meaning that the fewer bit-width, the less consumption in energy and memory. There has been a growing attention towards these techniques. For example, the computation time and energy of BISMO [62, 63] is linearly proportional to the bitwidth of input operands. Bit Fusion [64] is a bit-flexible accelerator, that constitutes an array of bit-level processing elements that dynamically fuse to match the bitwidth of individual DNN layers. For VGG-7 on CIFAR10, Bit Fusion consumes 895 milliwatts, which is two orders of magnitude lower than a 250-Watt Titan Xp that uses 8-bit computations.

There are also studies for efficient memory in variable bit-width. The representative research ShapeShifter [65] suggested that a smart encoding and decoding scheme can mitigate memory alignment issues and can saves up to 80% bandwidth/memory. More importantly, it can seamlessly cooperate with BISMO and Bit Fusion architecture. The overhead introduced by this technique is trivial compares to the benefits and opportunity it brings to us. Hardware with such techniques facilitates in-situ learning for resource constrained edge AI/ML.

### 5.2 Distribution of Bitwidth

Figure 7 shows the distribution of bitwidth for ShuffleNetV2 on ImageNet. The light color implies quantisation underflow happens more often in the `branch_main.3` of each basic unit at the beginning of training. In the second half of the training process, the bitwidth of these layers drop slightly, which suggests underflow happens less often. Other models and datasets have rather different distribution of bitwidth. Please refer to Appendix for more details.

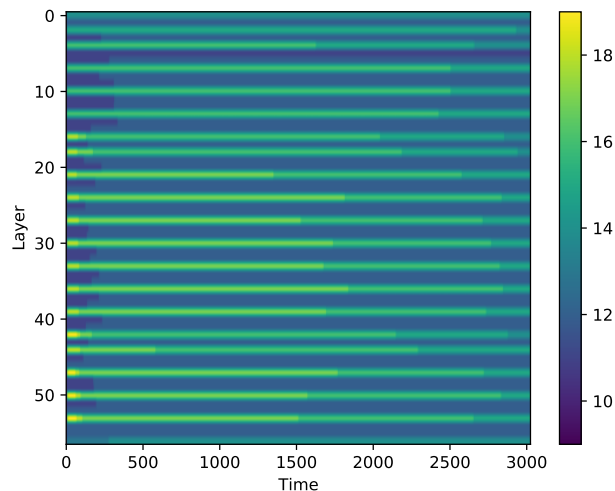


Figure 7: ShuffleNetV2 on ImageNet, history of bitwidth. x-axis stands for time, y-axis stands for different layers. First layer is at the top. Each time tick represents 100 steps

### 5.3 Bitwidth v.s. Batch Size

Larger batch size leads to larger gradients and less frequent quantisation underflow. That means a model can learn effectively with lower bitwidth. Please refer to Appendix for detailed experiment on this feature of RCT.

In many edge applications, the batch size of training data is usually quite limited. *micro-batching* [66] is one of methods that can mitigate the limitation in batch size. It is also known as *Gradient Accumulation*, which is widely adopted by NLP research community. This method accumulates gradients from multiple batches before carrying out model update. With this technique, RCT can have larger gradients and lower quantisation underflow, which leads to models with lower bitwidth.

## 6 Conclusion

In-situ training for resource constrained edge AI is challenging. We propose Resource Constrained Training method that saves both energy cost and memory usage for training. RCT evaluates how effective each layer learns with its current precision. Based on the evaluation, RCT performs per-layer bitwidth adjustments dynamically to make sure the model learns effective throughout the training process. We evaluate RCT with image classification and NLP tasks. Results suggest that RCT effectively saves memory and energy for training, without compromising the accuracy of a model.

## References

- [1] Jiasi Chen and Xukan Ran. Deep learning with edge computing: A review. *Proceedings of the IEEE*, 107(8):1655–1674, 2019.
- [2] Alex Krizhevsky, Ilya Sutskever, and Geoffrey E Hinton. Imagenet classification with deep convolutional neural networks. In *Advances in neural information processing systems*, pages 1097–1105, 2012.
- [3] Geoffrey Hinton, Li Deng, Dong Yu, George E Dahl, Abdel-rahman Mohamed, Navdeep Jaitly, Andrew Senior, Vincent Vanhoucke, Patrick Nguyen, Tara N Sainath, et al. Deep neural networks for acoustic modeling in speech recognition: The shared views of four research groups. *IEEE Signal processing magazine*, 29(6):82–97, 2012.
- [4] David Silver, Aja Huang, Chris J Maddison, Arthur Guez, Laurent Sifre, George Van Den Driessche, Julian Schrittwieser, Ioannis Antonoglou, Veda Panneershelvam, Marc Lanctot, et al. Mastering the game of go with deep neural networks and tree search. *nature*, 529(7587):484, 2016.
- [5] Raghuraman Krishnamoorthi. Quantizing deep convolutional networks for efficient inference: A whitepaper. *arXiv preprint arXiv:1806.08342*, 2018.
- [6] Moran Shkolnik, Brian Chmiel, Ron Banner, Gil Shomron, Yuri Nahshan, Alex Bronstein, and Uri Weiser. Robust quantization: One model to rule them all. *arXiv preprint arXiv:2002.07686*, 2020.
- [7] Ruihao Gong, Xianglong Liu, Shenghu Jiang, Tianxiang Li, Peng Hu, Jiazhen Lin, Fengwei Yu, and Junjie Yan. Differentiable soft quantization: Bridging full-precision and low-bit neural networks. In *Proceedings of the IEEE/CVF International Conference on Computer Vision*, pages 4852–4861, 2019.
- [8] Qing Jin, Linjie Yang, and Zhenyu Liao. Towards efficient training for neural network quantization. *arXiv preprint arXiv:1912.10207*, 2019.
- [9] Jiwei Yang, Xu Shen, Jun Xing, Xinmei Tian, Houqiang Li, Bing Deng, Jianqiang Huang, and Xian-sheng Hua. Quantization networks. In *The IEEE Conference on Computer Vision and Pattern Recognition (CVPR)*, June 2019.
- [10] Chaim Baskin, Natan Liss, Yoav Chai, Evgenii Zheltonozhskii, Eli Schwartz, Raja Giryes, Avi Mendelson, and Alexander M Bronstein. Nice: Noise injection and clamping estimation for neural network quantization. *arXiv preprint arXiv:1810.00162*, 2018.
- [11] Dongqing Zhang, Jiaolong Yang, Dongqiangzi Ye, and Gang Hua. Lq-nets: Learned quantization for highly accurate and compact deep neural networks. In *Proceedings of the European conference on computer vision (ECCV)*, pages 365–382, 2018.
- [12] Fengfu Li, Bo Zhang, and Bin Liu. Ternary weight networks. *arXiv preprint arXiv:1605.04711*, 2016.
- [13] Haoli Bai, Wei Zhang, Lu Hou, Lifeng Shang, Jing Jin, Xin Jiang, Qun Liu, Michael Lyu, and Irwin King. Binarybert: Pushing the limit of bert quantization. *arXiv preprint arXiv:2012.15701*, 2020.
- [14] Hyungjun Kim, Kyungsu Kim, Jinseok Kim, and Jae-Joon Kim. Binaryduo: Reducing gradient mismatch in binary activation network by coupling binary activations. *arXiv preprint arXiv:2002.06517*, 2020.
- [15] Chunlei Liu, Wenrui Ding, Xin Xia, Yuan Hu, Baochang Zhang, Jianzhuang Liu, Bohan Zhuang, and Guodong Guo. Rbcn: Rectified binary convolutional networks for enhancing the performance of 1-bit dnn. *arXiv preprint arXiv:1908.07748*, 2019.
- [16] Hanyu Peng and Shifeng Chen. Bdcnn: Binary convolution neural networks for fast object detection. *Pattern Recognition Letters*, 125:91–97, 2019.

- [17] Mohammad Rastegari, Vicente Ordonez, Joseph Redmon, and Ali Farhadi. Xnor-net: Imagenet classification using binary convolutional neural networks. In *European conference on computer vision*, pages 525–542. Springer, 2016.
- [18] Shuchang Zhou, Yuxin Wu, Zekun Ni, Xinyu Zhou, He Wen, and Yuheng Zou. Dorefa-net: Training low bitwidth convolutional neural networks with low bitwidth gradients. *arXiv preprint arXiv:1606.06160*, 2016.
- [19] Paulius Micikevicius, Sharan Narang, Jonah Alben, Gregory Diamos, Erich Elsen, David Garcia, Boris Ginsburg, Michael Houston, Oleksii Kuchaiev, Ganesh Venkatesh, et al. Mixed precision training. *arXiv preprint arXiv:1710.03740*, 2017.
- [20] Ron Banner, Itay Hubara, Elad Hoffer, and Daniel Soudry. Scalable methods for 8-bit training of neural networks. *arXiv preprint arXiv:1805.11046*, 2018.
- [21] Shuang Wu, Guoqi Li, Feng Chen, and Luping Shi. Training and inference with integers in deep neural networks. *arXiv preprint arXiv:1802.04680*, 2018.
- [22] Yukuan Yang, Lei Deng, Shuang Wu, Tianyi Yan, Yuan Xie, and Guoqi Li. Training high-performance and large-scale deep neural networks with full 8-bit integers. *Neural Networks*, 125:70–82, 2020.
- [23] Ofir Zafir, Guy Boudoukh, Peter Izsak, and Moshe Wasserblat. Q8bert: Quantized 8bit bert. *arXiv preprint arXiv:1910.06188*, 2019.
- [24] Sehoon Kim, Amir Gholami, Zhewei Yao, Michael W Mahoney, and Kurt Keutzer. I-bert: Integer-only bert quantization. *arXiv preprint arXiv:2101.01321*, 2021.
- [25] Bichen Wu, Yanghan Wang, Peizhao Zhang, Yuandong Tian, Peter Vajda, and Kurt Keutzer. Mixed precision quantization of convnets via differentiable neural architecture search. *arXiv preprint arXiv:1812.00090*, 2018.
- [26] Kuan Wang, Zhijian Liu, Yujun Lin, Ji Lin, and Song Han. Haq: Hardware-aware automated quantization with mixed precision. In *Proceedings of the IEEE conference on computer vision and pattern recognition*, pages 8612–8620, 2019.
- [27] Sheng Shen, Zhen Dong, Jiayu Ye, Linjian Ma, Zhewei Yao, Amir Gholami, Michael W Mahoney, and Kurt Keutzer. Q-bert: Hessian based ultra low precision quantization of bert. In *Proceedings of the AAAI Conference on Artificial Intelligence*, volume 34, pages 8815–8821, 2020.
- [28] Yiren Zhou, Seyed-Mohsen Moosavi-Dezfooli, Ngai-Man Cheung, and Pascal Frossard. Adaptive quantization for deep neural network. In *Thirty-Second AAAI Conference on Artificial Intelligence*, 2018.
- [29] Jiong Gong, Haihao Shen, Guoming Zhang, Xiaoli Liu, Shane Li, Ge Jin, Niharika Maheshwari, Evarist Fomenko, and Eden Segal. Highly efficient 8-bit low precision inference of convolutional neural networks with intelcaffe. In *Proceedings of the 1st on Reproducible Quality-Efficient Systems Tournament on Co-designing Pareto-efficient Deep Learning*, page 1. 2018.
- [30] Naveen Mellempudi, Abhisek Kundu, Dheevatsa Mudigere, Dipankar Das, Bharat Kaul, and Pradeep Dubey. Ternary neural networks with fine-grained quantization. *arXiv preprint arXiv:1705.01462*, 2017.
- [31] Yoni Choukroun, Eli Kravchik, Fan Yang, and Pavel Kisilev. Low-bit quantization of neural networks for efficient inference. In *ICCV Workshops*, pages 3009–3018, 2019.
- [32] Prateeth Nayak, David Zhang, and Sek Chai. Bit efficient quantization for deep neural networks. *arXiv preprint arXiv:1910.04877*, 2019.
- [33] Jun Fang, Ali Shafiee, Hamzah Abdel-Aziz, David Thorsley, Georgios Georgiadis, and Joseph Hassoun. Near-lossless post-training quantization of deep neural networks via a piecewise linear approximation. *arXiv preprint arXiv:2002.00104*, 2020.
- [34] Ali Hadi Zadeh, Isak Edo, Omar Mohamed Awad, and Andreas Moshovos. Gobo: Quantizing attention-based nlp models for low latency and energy efficient inference. In *2020 53rd Annual IEEE/ACM International Symposium on Microarchitecture (MICRO)*, pages 811–824. IEEE, 2020.
- [35] Song Han, Huizi Mao, and William J Dally. Deep compression: Compressing deep neural networks with pruning, trained quantization and huffman coding. *arXiv preprint arXiv:1510.00149*, 2015.
- [36] Jonathan Frankle and Michael Carbin. The lottery ticket hypothesis: Finding sparse, trainable neural networks. *arXiv preprint arXiv:1803.03635*, 2018.
- [37] Tim Dettmers and Luke Zettlemoyer. Sparse networks from scratch: Faster training without losing performance. *arXiv preprint arXiv:1907.04840*, 2019.
- [38] Trevor Gale, Erich Elsen, and Sara Hooker. The state of sparsity in deep neural networks. february 2019. *URL <http://arxiv.org/abs>*, 1902.

- [39] Zhuang Liu, Mingjie Sun, Tinghui Zhou, Gao Huang, and Trevor Darrell. Rethinking the value of network pruning. *arXiv preprint arXiv:1810.05270*, 2018.
- [40] Kaiyuan Guo, Shulin Zeng, Jincheng Yu, Yu Wang, and Huazhong Yang. A survey of fpga-based neural network accelerator. *arXiv preprint arXiv:1712.08934*, 2017.
- [41] Nimit Sharad Sohoni, Christopher Richard Aberger, Megan Leszczynski, Jian Zhang, and Christopher Ré. Low-memory neural network training: A technical report. *arXiv preprint arXiv:1904.10631*, 2019.
- [42] Jianping Gou, Baosheng Yu, Stephen John Maybank, and Dacheng Tao. Knowledge distillation: A survey. *arXiv preprint arXiv:2006.05525*, 2020.
- [43] Tara N Sainath, Brian Kingsbury, Vikas Sindhwani, Ebru Arisoy, and Bhuvana Ramabhadran. Low-rank matrix factorization for deep neural network training with high-dimensional output targets. In *2013 IEEE international conference on acoustics, speech and signal processing*, pages 6655–6659. IEEE, 2013.
- [44] Chong Li and CJ Richard Shi. Constrained optimization based low-rank approximation of deep neural networks. In *Proceedings of the European Conference on Computer Vision (ECCV)*, pages 732–747, 2018.
- [45] Chi Zhang and Viktor Prasanna. Frequency domain acceleration of convolutional neural networks on cpu-fpga shared memory system. In *Proceedings of the 2017 ACM/SIGDA International Symposium on Field-Programmable Gate Arrays*, pages 35–44, 2017.
- [46] Benoit Jacob, Skirmantas Kligys, Bo Chen, Menglong Zhu, Matthew Tang, Andrew Howard, Hartwig Adam, and Dmitry Kalenichenko. Quantization and training of neural networks for efficient integer-arithmetic-only inference. In *Proceedings of the IEEE Conference on Computer Vision and Pattern Recognition*, pages 2704–2713, 2018.
- [47] Suyog Gupta, Ankur Agrawal, Kailash Gopalakrishnan, and Pritish Narayanan. Deep learning with limited numerical precision. In *International Conference on Machine Learning*, pages 1737–1746, 2015.
- [48] Mark Horowitz. 1.1 computing’s energy problem (and what we can do about it). In *2014 IEEE International Solid-State Circuits Conference Digest of Technical Papers (ISSCC)*, pages 10–14. IEEE, 2014.
- [49] Alex Krizhevsky, Geoffrey Hinton, et al. Learning multiple layers of features from tiny images. 2009.
- [50] Yuval Netzer, Tao Wang, Adam Coates, Alessandro Bissacco, Bo Wu, and Andrew Ng. Reading digits in natural images with unsupervised feature learning. *NIPS*, 01 2011.
- [51] Jia Deng, Wei Dong, Richard Socher, Li-Jia Li, Kai Li, and Li Fei-Fei. Imagenet: A large-scale hierarchical image database. In *2009 IEEE conference on computer vision and pattern recognition*, pages 248–255. Ieee, 2009.
- [52] Kaiming He, Xiangyu Zhang, Shaoqing Ren, and Jian Sun. Deep residual learning for image recognition. In *Proceedings of the IEEE conference on computer vision and pattern recognition*, pages 770–778, 2016.
- [53] Mark Sandler, Andrew Howard, Menglong Zhu, Andrey Zhmoginov, and Liang-Chieh Chen. Mobilenetv2: Inverted residuals and linear bottlenecks. In *Proceedings of the IEEE conference on computer vision and pattern recognition*, pages 4510–4520, 2018.
- [54] Sergey Zagoruyko and Nikos Komodakis. Wide residual networks. *arXiv preprint arXiv:1605.07146*, 2016.
- [55] Terrance DeVries and Graham W Taylor. Improved regularization of convolutional neural networks with cutout. *arXiv preprint arXiv:1708.04552*, 2017.
- [56] Yanping Huang, Youlong Cheng, Ankur Bapna, Orhan Firat, Dehao Chen, Mia Chen, HyounJoong Lee, Jiquan Ngiam, Quoc V Le, Yonghui Wu, et al. Gpipe: Efficient training of giant neural networks using pipeline parallelism. In *Advances in neural information processing systems*, pages 103–112, 2019.
- [57] Ashish Vaswani, Noam Shazeer, Niki Parmar, Jakob Uszkoreit, Llion Jones, Aidan N Gomez, Lukasz Kaiser, and Illia Polosukhin. Attention is all you need. *arXiv preprint arXiv:1706.03762*, 2017.
- [58] Jacob Devlin, Ming-Wei Chang, Kenton Lee, and Kristina Toutanova. Bert: Pre-training of deep bidirectional transformers for language understanding. *arXiv preprint arXiv:1810.04805*, 2018.
- [59] Alex Wang, Amanpreet Singh, Julian Michael, Felix Hill, Omer Levy, and Samuel R Bowman. Glue: A multi-task benchmark and analysis platform for natural language understanding. *arXiv preprint arXiv:1804.07461*, 2018.
- [60] Pranav Rajpurkar, Jian Zhang, Konstantin Lopyrev, and Percy Liang. Squad: 100,000+ questions for machine comprehension of text. *arXiv preprint arXiv:1606.05250*, 2016.
- [61] Yichi Zhang, Ritchie Zhao, Weizhe Hua, Nayun Xu, G. Edward Suh, and Zhiru Zhang. Precision gating: Improving neural network efficiency with dynamic dual-precision activations. In *International Conference on Learning Representations*, 2020.

- 
- [62] Patrick Judd, Jorge Albericio, Tayler Hetherington, Tor M Aamodt, and Andreas Moshovos. Stripes: Bit-serial deep neural network computing. In *2016 49th Annual IEEE/ACM International Symposium on Microarchitecture (MICRO)*, pages 1–12. IEEE, 2016.
- [63] Yaman Umuroglu, Lahiru Rasnayake, and Magnus Sjölander. Bismo: A scalable bit-serial matrix multiplication overlay for reconfigurable computing. In *2018 28th International Conference on Field Programmable Logic and Applications (FPL)*, pages 307–3077. IEEE, 2018.
- [64] Hardik Sharma, Jongse Park, Naveen Suda, Liangzhen Lai, Benson Chau, Vikas Chandra, and Hadi Esmaeilzadeh. Bit fusion: Bit-level dynamically composable architecture for accelerating deep neural network. In *2018 ACM/IEEE 45th Annual International Symposium on Computer Architecture (ISCA)*, pages 764–775. IEEE, 2018.
- [65] Alberto Delmás Lascorz, Sayeh Sharify, Isak Edo, Dylan Malone Stuart, Omar Mohamed Awad, Patrick Judd, Mostafa Mahmoud, Milos Nikolic, Kevin Siu, Zissis Poulos, et al. Shapeshifter: Enabling fine-grain data width adaptation in deep learning. In *Proceedings of the 52nd Annual IEEE/ACM International Symposium on Microarchitecture*, pages 28–41, 2019.
- [66] Yanping Huang, Youlong Cheng, Ankur Bapna, Orhan Firat, Mia Xu Chen, Dehao Chen, HyoukJoong Lee, Jiquan Ngiam, Quoc V Le, Yonghui Wu, et al. Gpipe: Efficient training of giant neural networks using pipeline parallelism. *arXiv preprint arXiv:1811.06965*, 2018.

# Appendices

## A Initialisation of Bitwidth

The accuracy at the end of training is not sensitive to the setting of the initial bitwidth. To prove this, we use RCT to train WideResNet-28-10 on SVHN with different settings of the initial bitwidth, ranging from 4-bit to 12-bit. For the rest of data augmentation and training setting we follow [54]. The results is shown in Fig.8.

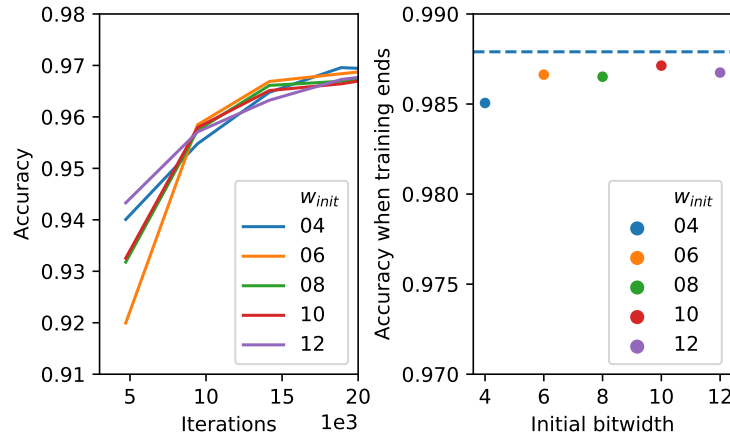


Figure 8: Accuracy v.s. different initial bitwidth

The left part of Fig.8 demonstrates the accuracy curve at the beginning of the training. Models with different initial bitwidth has different starting accuracy at the first first epoch. The divergence gradually narrows, because RCT is allocating more bitwidth to models with fewer initial bitwidth. The right part of the figure shows the accuracy at the end of the training achieved by these models. All the points are very close to the dashed line, which represents the accuracy achieved by floating-point training. This experiment suggests that the RCT is not sensitive to the initial bitwidth. Therefore we will use initial bitwidth of 8-bit for the rest of the experiments

We then demonstrate that, starting with low-precision model, RCT can catch up with the progress of floating-point training. We follow the training settings in [52] Fig.9 shows the first few epochs of the training progress of ResNet-20 on CIFAR10.

FP32 and 16-bit model has the steepest learning curves among all, as they do not suffer much from quantisation underflow problem. The curve of 8-bit model does not climb as fast as FP32 and 16-bit does. An investigation into the training statistics shows that  $G_{avg}$  of the all layers drop from the scale of 1 down to  $1e-1$  within the first 50 epoch, which indicates quantisation underflow happens model wide and significantly slows down the training process of the 8-bit model. On comparison, RCT starts with a model initialised with 8-bit weights. Its training curve starts with lower accuracy at the beginning. It overtakes the 8-bit and catch up with 16-bit and FP32.

## B Bitwidth v.s. Batch Size

Figure 10 shows the relation between batch size and bitwidth for BERT on SQuADv1.1. This figure suggests that larger batch size leads to lower bitwidth. This is because quantisation underflow happens less often if the gradient is larger. The batch size for language model is much smaller than that for CNN models. For example, batch size is 12 for BERT on SQuADv1.1 and 1024 for ShuffleNetV2 on ImageNet. This explain why the averaged bitwidth for language model is a few bits higher than that for CNN models.

## C Distribution of Bitwidth Over Time

### C.1 ResNet-18 on Imagenet

Table 3: ResNet-18 on Imagenet, bitwidth at last step

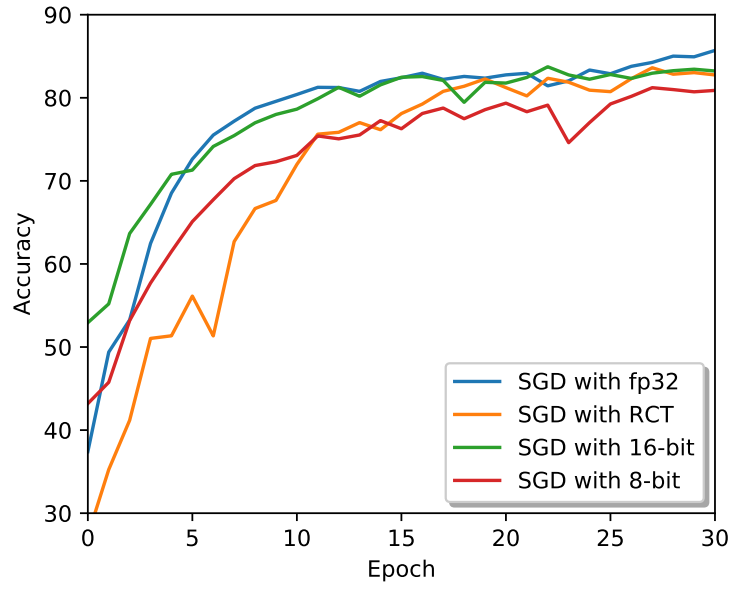


Figure 9: Test Accuracy v.s. Epoch for ResNet20 on CIFAR10

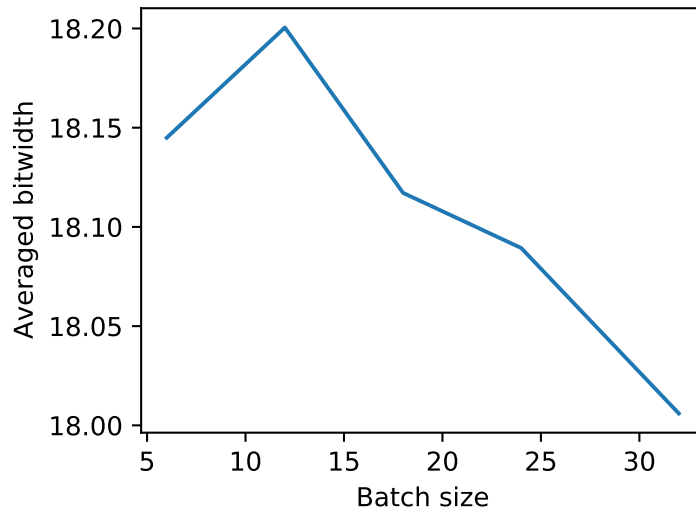


Figure 10: BERT on SQuADv1.1, batch size v.s. bitwidth. x-axis stands for batch size, y-axis is the averaged bitwidth at the end of RCT training.

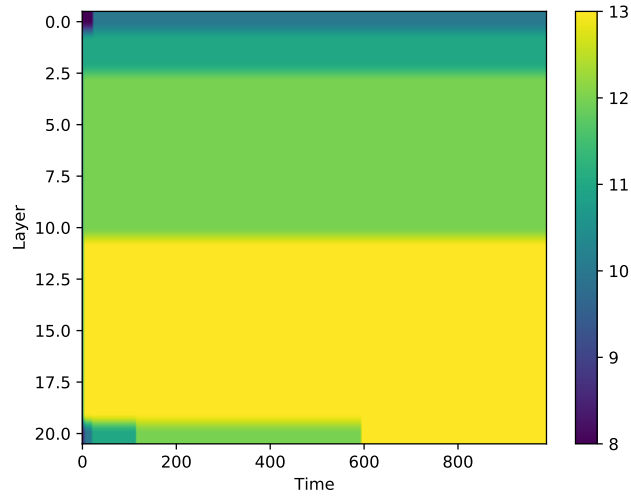


Figure 11: ResNet-18 on ImageNet, history of bitwidth. x-axis stands for time, y-axis stands for different layers. First layer is at the top. Each time tick represents 500 steps

| Layer name            | Bitwidth |
|-----------------------|----------|
| conv1                 | 10.0     |
| layer1.0.conv1        | 11.0     |
| layer1.0.conv2        | 11.0     |
| layer1.1.conv1        | 12.0     |
| layer1.1.conv2        | 12.0     |
| layer2.0.conv1        | 12.0     |
| layer2.0.conv2        | 12.0     |
| layer2.0.downsample.0 | 12.0     |
| layer2.1.conv1        | 12.0     |
| layer2.1.conv2        | 12.0     |
| layer3.0.conv1        | 12.0     |
| layer3.0.conv2        | 13.0     |
| layer3.0.downsample.0 | 13.0     |
| layer3.1.conv1        | 13.0     |
| layer3.1.conv2        | 13.0     |
| layer4.0.conv1        | 13.0     |
| layer4.0.conv2        | 13.0     |
| layer4.0.downsample.0 | 13.0     |
| layer4.1.conv1        | 13.0     |
| layer4.1.conv2        | 13.0     |
| fc                    | 13.0     |

## C.2 ShuffleNetV2 on Imagenet

Table 4: ShuffleNetV2 on ImageNet, bitwidth at last step

| Layer name               | Bitwidth |
|--------------------------|----------|
| first_conv.0             | 14.0     |
| features.0.branch_main.0 | 12.0     |
| features.0.branch_main.3 | 14.0     |
| features.0.branch_main.5 | 12.0     |
| features.0.branch_proj.0 | 14.0     |

*continued on next page*

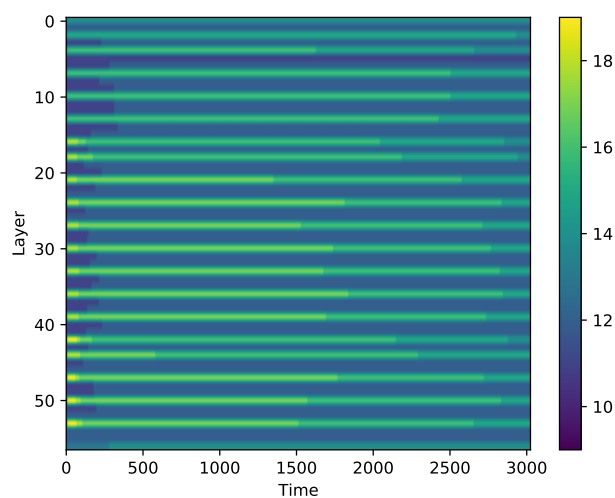


Figure 12: ShuffleNetV2 on ImageNet, history of bitwidth. x-axis stands for time, y-axis stands for different layers. First layer is at the top. Each time tick represents 100 steps

*continued from previous page*

| Layer name                | Bitwidth |
|---------------------------|----------|
| features.0.branch_proj.2  | 11.0     |
| features.1.branch_main.0  | 12.0     |
| features.1.branch_main.3  | 15.0     |
| features.1.branch_main.5  | 12.0     |
| features.2.branch_main.0  | 12.0     |
| features.2.branch_main.3  | 15.0     |
| features.2.branch_main.5  | 12.0     |
| features.3.branch_main.0  | 12.0     |
| features.3.branch_main.3  | 15.0     |
| features.3.branch_main.5  | 12.0     |
| features.4.branch_main.0  | 12.0     |
| features.4.branch_main.3  | 14.0     |
| features.4.branch_main.5  | 12.0     |
| features.4.branch_proj.0  | 14.0     |
| features.4.branch_proj.2  | 12.0     |
| features.5.branch_main.0  | 12.0     |
| features.5.branch_main.3  | 15.0     |
| features.5.branch_main.5  | 12.0     |
| features.6.branch_main.0  | 12.0     |
| features.6.branch_main.3  | 15.0     |
| features.6.branch_main.5  | 12.0     |
| features.7.branch_main.0  | 12.0     |
| features.7.branch_main.3  | 15.0     |
| features.7.branch_main.5  | 12.0     |
| features.8.branch_main.0  | 12.0     |
| features.8.branch_main.3  | 15.0     |
| features.8.branch_main.5  | 12.0     |
| features.9.branch_main.0  | 12.0     |
| features.9.branch_main.3  | 15.0     |
| features.9.branch_main.5  | 12.0     |
| features.10.branch_main.0 | 12.0     |
| features.10.branch_main.3 | 15.0     |

*continued on next page*

*continued from previous page*

| Layer name                | Bitwidth |
|---------------------------|----------|
| features.10.branch_main.5 | 12.0     |
| features.11.branch_main.0 | 12.0     |
| features.11.branch_main.3 | 15.0     |
| features.11.branch_main.5 | 12.0     |
| features.12.branch_main.0 | 12.0     |
| features.12.branch_main.3 | 14.0     |
| features.12.branch_main.5 | 12.0     |
| features.12.branch_proj.0 | 15.0     |
| features.12.branch_proj.2 | 12.0     |
| features.13.branch_main.0 | 12.0     |
| features.13.branch_main.3 | 15.0     |
| features.13.branch_main.5 | 12.0     |
| features.14.branch_main.0 | 12.0     |
| features.14.branch_main.3 | 15.0     |
| features.14.branch_main.5 | 12.0     |
| features.15.branch_main.0 | 12.0     |
| features.15.branch_main.3 | 15.0     |
| features.15.branch_main.5 | 12.0     |
| conv_last.0               | 12.0     |
| classifier.0              | 14.0     |

### C.3 BERT on MRPC

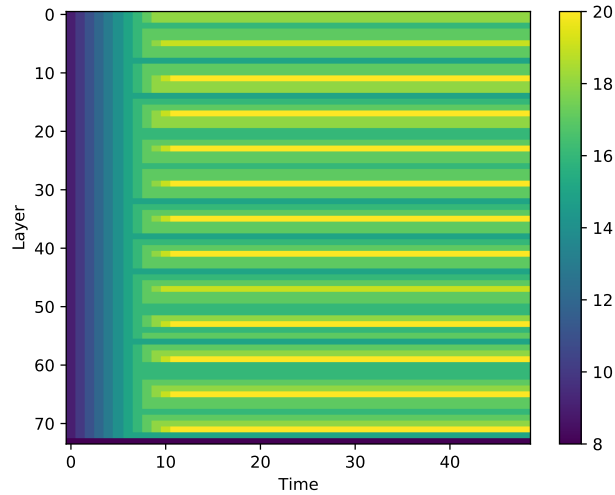


Figure 13: BERT on MRPC, history of bitwidth. x-axis stands for time, y-axis stands for different layers. First layer is at the top. Each time tick represents 23 steps

Table 5: BERT on MRPC, bitwidth at last step

| Layer name                                  | Bitwidth |
|---|----------|
| bert.encoder.layer.0.attention.self.query   | 18.0     |
| bert.encoder.layer.0.attention.self.key     | 18.0     |
| bert.encoder.layer.0.attention.self.value   | 16.0     |
| bert.encoder.layer.0.attention.output.dense | 17.0     |

*continued on next page*

*continued from previous page*

| Layer name                                  | Bitwidth |
|---|----------|
| bert.encoder.layer.0.intermediate.dense     | 17.0     |
| bert.encoder.layer.0.output.dense           | 19.0     |
| bert.encoder.layer.1.attention.self.query   | 17.0     |
| bert.encoder.layer.1.attention.self.key     | 17.0     |
| bert.encoder.layer.1.attention.self.value   | 15.0     |
| bert.encoder.layer.1.attention.output.dense | 17.0     |
| bert.encoder.layer.1.intermediate.dense     | 17.0     |
| bert.encoder.layer.1.output.dense           | 20.0     |
| bert.encoder.layer.2.attention.self.query   | 18.0     |
| bert.encoder.layer.2.attention.self.key     | 18.0     |
| bert.encoder.layer.2.attention.self.value   | 15.0     |
| bert.encoder.layer.2.attention.output.dense | 16.0     |
| bert.encoder.layer.2.intermediate.dense     | 17.0     |
| bert.encoder.layer.2.output.dense           | 20.0     |
| bert.encoder.layer.3.attention.self.query   | 18.0     |
| bert.encoder.layer.3.attention.self.key     | 18.0     |
| bert.encoder.layer.3.attention.self.value   | 16.0     |
| bert.encoder.layer.3.attention.output.dense | 16.0     |
| bert.encoder.layer.3.intermediate.dense     | 17.0     |
| bert.encoder.layer.3.output.dense           | 20.0     |
| bert.encoder.layer.4.attention.self.query   | 17.0     |
| bert.encoder.layer.4.attention.self.key     | 17.0     |
| bert.encoder.layer.4.attention.self.value   | 16.0     |
| bert.encoder.layer.4.attention.output.dense | 17.0     |
| bert.encoder.layer.4.intermediate.dense     | 17.0     |
| bert.encoder.layer.4.output.dense           | 20.0     |
| bert.encoder.layer.5.attention.self.query   | 17.0     |
| bert.encoder.layer.5.attention.self.key     | 17.0     |
| bert.encoder.layer.5.attention.self.value   | 15.0     |
| bert.encoder.layer.5.attention.output.dense | 16.0     |
| bert.encoder.layer.5.intermediate.dense     | 17.0     |
| bert.encoder.layer.5.output.dense           | 20.0     |
| bert.encoder.layer.6.attention.self.query   | 17.0     |
| bert.encoder.layer.6.attention.self.key     | 17.0     |
| bert.encoder.layer.6.attention.self.value   | 15.0     |
| bert.encoder.layer.6.attention.output.dense | 16.0     |
| bert.encoder.layer.6.intermediate.dense     | 17.0     |
| bert.encoder.layer.6.output.dense           | 20.0     |
| bert.encoder.layer.7.attention.self.query   | 17.0     |
| bert.encoder.layer.7.attention.self.key     | 17.0     |
| bert.encoder.layer.7.attention.self.value   | 15.0     |
| bert.encoder.layer.7.attention.output.dense | 16.0     |
| bert.encoder.layer.7.intermediate.dense     | 17.0     |
| bert.encoder.layer.7.output.dense           | 19.0     |
| bert.encoder.layer.8.attention.self.query   | 17.0     |
| bert.encoder.layer.8.attention.self.key     | 17.0     |
| bert.encoder.layer.8.attention.self.value   | 16.0     |
| bert.encoder.layer.8.attention.output.dense | 16.0     |
| bert.encoder.layer.8.intermediate.dense     | 18.0     |
| bert.encoder.layer.8.output.dense           | 20.0     |
| bert.encoder.layer.9.attention.self.query   | 16.0     |
| bert.encoder.layer.9.attention.self.key     | 17.0     |
| bert.encoder.layer.9.attention.self.value   | 15.0     |
| bert.encoder.layer.9.attention.output.dense | 17.0     |
| bert.encoder.layer.9.intermediate.dense     | 18.0     |
| bert.encoder.layer.9.output.dense           | 20.0     |

*continued on next page*

*continued from previous page*

| Layer name                                   | Bitwidth |
|--|----------|
| bert.encoder.layer.10.attention.self.query   | 16.0     |
| bert.encoder.layer.10.attention.self.key     | 16.0     |
| bert.encoder.layer.10.attention.self.value   | 16.0     |
| bert.encoder.layer.10.attention.output.dense | 17.0     |
| bert.encoder.layer.10.intermediate.dense     | 18.0     |
| bert.encoder.layer.10.output.dense           | 20.0     |
| bert.encoder.layer.11.attention.self.query   | 17.0     |
| bert.encoder.layer.11.attention.self.key     | 17.0     |
| bert.encoder.layer.11.attention.self.value   | 16.0     |
| bert.encoder.layer.11.attention.output.dense | 17.0     |
| bert.encoder.layer.11.intermediate.dense     | 18.0     |
| bert.encoder.layer.11.output.dense           | 20.0     |
| bert.pooler.dense                            | 15.0     |
| classifier                                   | 8.0      |

#### C.4 BERT on SQUADv1.1

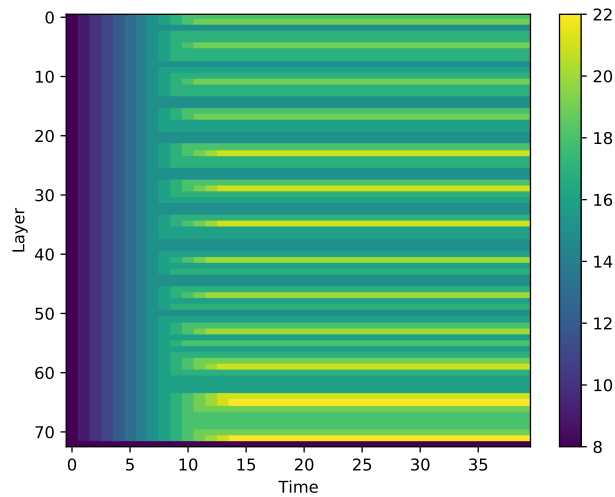


Figure 14: BERT on SQUADv1.1, history of bitwidth. x-axis stands for time, y-axis stands for different layers. First layer is at the top. Each time tick represents 369 steps

Table 6: BERT on SQUADv1.1, bitwidth at last step

| Layer name                                  | Bitwidth |
|---|----------|
| bert.encoder.layer.0.attention.self.query   | 18.0     |
| bert.encoder.layer.0.attention.self.key     | 19.0     |
| bert.encoder.layer.0.attention.self.value   | 15.0     |
| bert.encoder.layer.0.attention.output.dense | 17.0     |
| bert.encoder.layer.0.intermediate.dense     | 17.0     |
| bert.encoder.layer.0.output.dense           | 19.0     |
| bert.encoder.layer.1.attention.self.query   | 17.0     |
| bert.encoder.layer.1.attention.self.key     | 17.0     |
| bert.encoder.layer.1.attention.self.value   | 15.0     |
| bert.encoder.layer.1.attention.output.dense | 16.0     |

*continued on next page*

*continued from previous page*

| Layer name                                   | Bitwidth |
|--|----------|
| bert.encoder.layer.1.intermediate.dense      | 17.0     |
| bert.encoder.layer.1.output.dense            | 19.0     |
| bert.encoder.layer.2.attention.self.query    | 17.0     |
| bert.encoder.layer.2.attention.self.key      | 17.0     |
| bert.encoder.layer.2.attention.self.value    | 15.0     |
| bert.encoder.layer.2.attention.output.dense  | 15.0     |
| bert.encoder.layer.2.intermediate.dense      | 18.0     |
| bert.encoder.layer.2.output.dense            | 19.0     |
| bert.encoder.layer.3.attention.self.query    | 16.0     |
| bert.encoder.layer.3.attention.self.key      | 16.0     |
| bert.encoder.layer.3.attention.self.value    | 15.0     |
| bert.encoder.layer.3.attention.output.dense  | 15.0     |
| bert.encoder.layer.3.intermediate.dense      | 18.0     |
| bert.encoder.layer.3.output.dense            | 21.0     |
| bert.encoder.layer.4.attention.self.query    | 17.0     |
| bert.encoder.layer.4.attention.self.key      | 17.0     |
| bert.encoder.layer.4.attention.self.value    | 15.0     |
| bert.encoder.layer.4.attention.output.dense  | 15.0     |
| bert.encoder.layer.4.intermediate.dense      | 18.0     |
| bert.encoder.layer.4.output.dense            | 21.0     |
| bert.encoder.layer.5.attention.self.query    | 17.0     |
| bert.encoder.layer.5.attention.self.key      | 16.0     |
| bert.encoder.layer.5.attention.self.value    | 15.0     |
| bert.encoder.layer.5.attention.output.dense  | 15.0     |
| bert.encoder.layer.5.intermediate.dense      | 17.0     |
| bert.encoder.layer.5.output.dense            | 21.0     |
| bert.encoder.layer.6.attention.self.query    | 16.0     |
| bert.encoder.layer.6.attention.self.key      | 16.0     |
| bert.encoder.layer.6.attention.self.value    | 15.0     |
| bert.encoder.layer.6.attention.output.dense  | 15.0     |
| bert.encoder.layer.6.intermediate.dense      | 16.0     |
| bert.encoder.layer.6.output.dense            | 20.0     |
| bert.encoder.layer.7.attention.self.query    | 16.0     |
| bert.encoder.layer.7.attention.self.key      | 17.0     |
| bert.encoder.layer.7.attention.self.value    | 15.0     |
| bert.encoder.layer.7.attention.output.dense  | 15.0     |
| bert.encoder.layer.7.intermediate.dense      | 17.0     |
| bert.encoder.layer.7.output.dense            | 20.0     |
| bert.encoder.layer.8.attention.self.query    | 16.0     |
| bert.encoder.layer.8.attention.self.key      | 17.0     |
| bert.encoder.layer.8.attention.self.value    | 15.0     |
| bert.encoder.layer.8.attention.output.dense  | 16.0     |
| bert.encoder.layer.8.intermediate.dense      | 18.0     |
| bert.encoder.layer.8.output.dense            | 20.0     |
| bert.encoder.layer.9.attention.self.query    | 16.0     |
| bert.encoder.layer.9.attention.self.key      | 18.0     |
| bert.encoder.layer.9.attention.self.value    | 16.0     |
| bert.encoder.layer.9.attention.output.dense  | 17.0     |
| bert.encoder.layer.9.intermediate.dense      | 19.0     |
| bert.encoder.layer.9.output.dense            | 21.0     |
| bert.encoder.layer.10.attention.self.query   | 17.0     |
| bert.encoder.layer.10.attention.self.key     | 16.0     |
| bert.encoder.layer.10.attention.self.value   | 16.0     |
| bert.encoder.layer.10.attention.output.dense | 16.0     |
| bert.encoder.layer.10.intermediate.dense     | 21.0     |
| bert.encoder.layer.10.output.dense           | 22.0     |

*continued on next page*

---

*continued from previous page*

| Layer name                                   | Bitwidth |
|--|----------|
| bert.encoder.layer.11.attention.self.query   | 19.0     |
| bert.encoder.layer.11.attention.self.key     | 18.0     |
| bert.encoder.layer.11.attention.self.value   | 18.0     |
| bert.encoder.layer.11.attention.output.dense | 18.0     |
| bert.encoder.layer.11.intermediate.dense     | 19.0     |
| bert.encoder.layer.11.output.dense           | 22.0     |
| qa_outputs                                   | 8.0      |

---